Modeling Approach for Analysis and Optimization of a Long-Duration Mars Airplane

Reuben R. Rohrschneider,[*] John R. Olds,[†] Robert D. Braun[†] and Virgil Hutchinson, Jr.[*]
Georgia Institute of Technology, Atlanta, GA, 30332-0150

Christopher A. Kuhl[‡]
NASA Langley Research Center, Hampton, VA, 23681

and

Stephen R. Steffes[§]
The Charles Stark Draper Laboratory, Inc., Cambridge, MA, 02139

The goal of this study was to determine the best system level modeling tool for the design of a long endurance Mars airplane mission, and to use this tool to determine the best configuration for the aircraft. The mission model was built in the design framework ModelCenter. User-driven fixed point iteration (FPI), optimizer based decomposition (OBD) and a hybrid method were implemented. Convergence difficulties were discovered in the OBD and hybrid methods. The user-driven FPI method produced the most reliable results, but required the most time. A combination of the hybrid and user-driven FPI methods were used to perform a technology study in which five different propulsion systems were examined: a bipropellant rocket, a battery powered propeller, a direct methanol fuel cell powered propeller, and beamed solar and microwave powered propeller systems. The direct methanol fuel cell proved to be the best onboard power system for a long endurance airplane and the solar beamed power system showed potential for indefinite flight.

Nomenclature

ARES	=	Aerial Regional-Scale Environmental Survey
C_3	=	hyperbolic excess velocity, km^2/s^2
DC	=	direct current
DMFC	=	direct methanol fuel cell
D_{pullup}	=	distance the airplane drops vertically while performing the pull-up maneuver, m
DSM	=	design structure matrix
FPI	=	fixed point iteration
gdalt	=	geodetic altitude above Mars, m
IPREP	=	Interplanetary Preprocessor
LCC	=	life cycle cost, $M FY04
MMH	=	mono-methyl hydrazine
n	=	load factor
NASA	=	National Aeronautics and Space Administration
NTO	=	nitrogen tetroxide
OBD	=	optimizer based decomposition
POST	=	Program to Optimize Simulated Trajectories
SQP	=	sequential quadratic programming

[*] Graduate Research Assistant, Aerospace Engineering, 270 Ferst Dr., AIAA Student Member.
[†] Associate Professor, Aerospace Engineering, 270 Ferst Dr., AIAA Associate Fellow.
[‡] Aerospace Engineer, Exploration Engineering Branch, Mail Stop 472, AIAA Member.
[§] Guidance and Navigation Analyst, Guidance and Navigation Division, 555 Technology, AIAA Student Member.

W_{folded} = folded width of the airplane, m
V_{cruise} = airplane cruise velocity, m/s
Vol_{subs} = volume of airplane subsystems, m^3
Vol_{fuse} = volume of airplane fuselage, m^3

I. Introduction

THE scientific utility of Mars aerial platforms for visual imaging, spectroscopy, paleomagnetics, radar sounding, and atmospheric measurements has been identified by several authors[1,2,3]. The airplane's ability to obtain high resolution data and cover a regional-scale distances give it an advantage over orbiters and landers. To fulfill the science mission the correct suite of instruments must be carried. For this study the ARES payload[4] will be adopted since a large amount of research has already been invested in this area. Table 1 shows the instruments carried and the payload requirements. The basic mission profile consists of launch directly into Mars transfer orbit, inter-planetary cruise, direct entry at Mars, mid-air airplane deployment, and aerial traverse. The traverse is performed at constant altitude from the time the airplane reaches level flight until the propellant runs out. The small time spent coasting to the ground at the end of the flight is not included. The science mission is conducted during the aerial traverse which places constraints on the airplane design. A diagram of the mission profile is shown in Figure 1.

Table 1. Science payload carried by ARES.

Instrument	Mass, kg	Power, W	Volume, cm^3
Magnetometer	1.15	0.6	635
Mass Spectrometer	4.74	6.4	3359
Point Spectrometer	3.54	16.0	24355
Context Camera	0.50	2.0	756
Video Camera	0.20	5.0	504
Totals	**10.13**	**30**	**29609 = 0.0296 m^3**

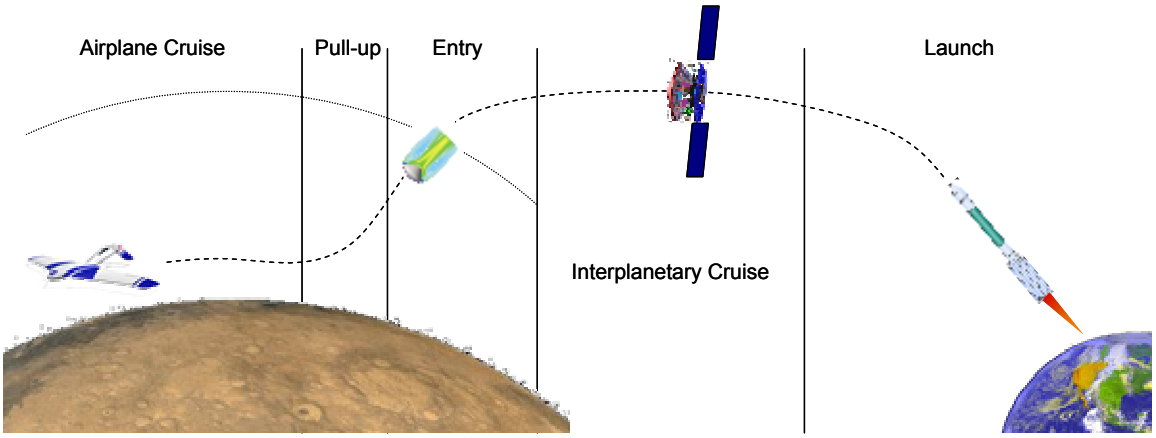

Figure 1. The Mars airplane mission profile.

The goal of the science mission is to obtain as many new measurements as possible during the flight. This can be achieved by either extending the range or endurance of the airplane, or by keeping the range and endurance fixed while increasing the payload. This study will focus on increasing the airplane endurance so that more data can be gathered. Endurance improvements can be made in two ways: by changing the technologies used, or by finding a combination of the design variables that produce a better solution. This study explores both of these methods. First an optimum solution will be sought for the baseline vehicle and the influence of vehicle size will be explored. The baseline vehicle will then be improved by applying different technologies and subsystems to the vehicle. For each technology investigated, a vehicle size study will be performed. This method ensures that all technologies are compared at their greatest potential for the given mission.

II. Model Description

The Mars airplane mission model consists of many different analyses that are broken down according to traditional disciplines. Figure 2 shows the contributing analyses assembled in a design structure matrix (DSM) for the full mission and a detail of the airplane model. In a DSM the analysis proceeds from the upper left to the lower right with data flow indicated by a circle at the intersection of lines connecting any two analyses. Strong links are indicated by solid circles, and weak links by open circles. Connections between the contributing analyses above the diagonal indicate forward flow of information, and lines below the diagonal indicate backward flow of information. A diagonal line across the analysis box indicates that the analysis includes a built-in optimizer. From this depiction of the model the necessary feedback loops are easily visible, and it can be seen that changing the order of the analyses cannot eliminate the feedback loops for this problem.

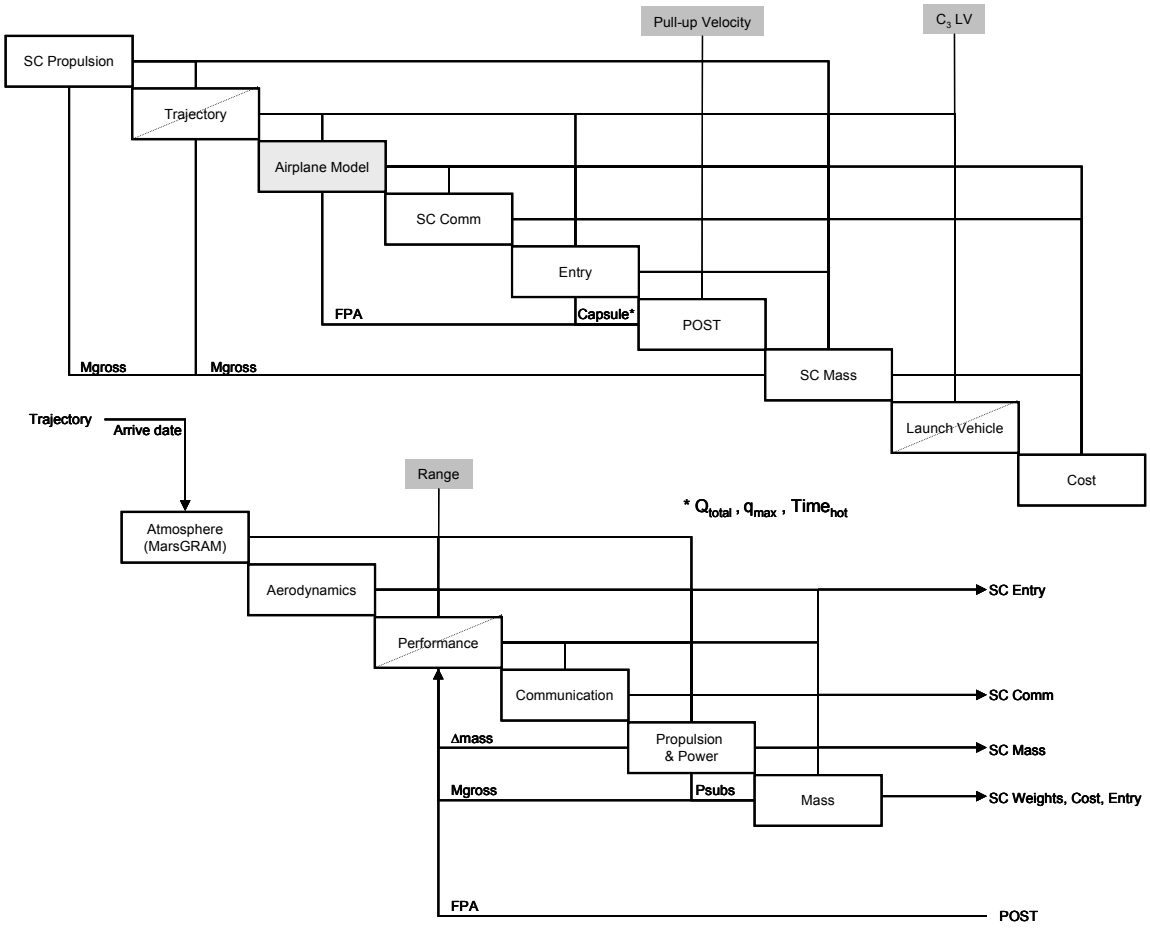

Figure 2. The Mars airplane mission analysis depicted in a DSM. The feedback links are shown and the feedback variables are labeled. Design variables controlled by the system level optimizer are shown in grey boxes.

Solution of problems with feedback loops requires a scheme that ensures consistency of the feedback variables. The most common method used is fixed point iteration (FPI) but other methods also exist, such as optimizer based decomposition (OBD). These methods require running each analysis repeatedly, which is time consuming and tedious if done by hand. In this analysis ModelCenter[5], a commercially available computational framework from Phoenix Integration, was employed. Figure 3 shows the Mars airplane mission model implemented in ModelCenter using FPI to converge the model and a generic optimizer to maximize airplane endurance.

The Mars airplane mission model consists of 14 contributing analyses. To familiarize the reader with the assumptions and limitations of the model, the method behind each contributing analysis will be described.

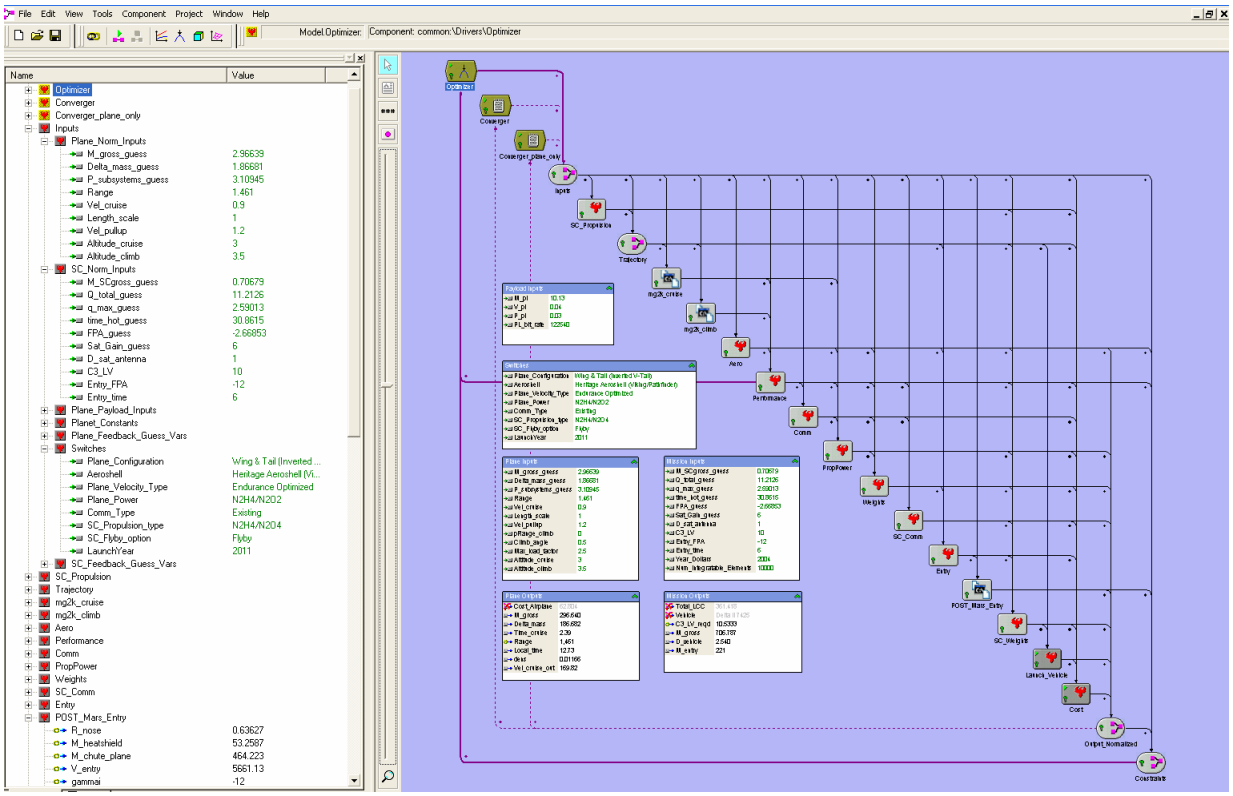

Figure 3. The Mars airplane model implemented in ModelCenter. Design variables are on the left, and a schematic of the model is in the main window.

A. Spacecraft Propulsion

The spacecraft propulsion system model sizes the main engine for the cruise stage. MMH/NTO bipropellant and MMH monopropellant rocket engines are sized using thrust required and a curve fit of rocket engine thrust to weight and dimensions[6]. Required thrust is determined by assuming a spacecraft thrust to weight of 1/10 so that instantaneous velocity changes can be assumed. The engine specific impulse, mass, and volume are output for use in the spacecraft mass analysis.

B. Interplanetary Trajectory

The trajectory from Earth to Mars was calculated using IPREP[7], a three dimensional patched conic method. IPREP was used to find the best two week launch window for each launch opportunity from 2005 until 2016. Outputs include arrival date at Mars, departure excess velocity, arrival excess velocity, required departure C_3, time of flight, and mass ratio required for the spacecraft to provide the required velocity change on departure and arrival. The departure mass ratio takes into account the C_3 capability of the launch vehicle. The final analysis consists of a table lookup with the required output data listed for each launch opportunity available.

C. Mars Atmosphere

The Mars atmosphere is modeled with Mars Global Reference Atmospheric Model 2000 to calculate the atmospheric conditions at the cruise and maximum climb altitudes for the airplane[8]. The model is used at its most basic level, and requires knowledge of only the arrival date, time, altitude and location on Mars. Here altitude is measured from the Mars reference ellipsoid, and no wave model is used. The dust optical density is set to 0.3, indicating a constant low dust level, consistent with current Mars mission standards.

D. Aerodynamics & Configuration

The aerodynamics and configuration model uses photographic scaling to resize the vehicle, which allows for simple scaling of the geometry, and fixed aerodynamic coefficients. Aircraft aerodynamic and configuration data is taken from previous studies where available. The baseline configuration is based on the ARES[9] study performed at NASA Langley Research Center.

E. Airplane Performance

The aerodynamic coefficients are fed into the performance model where the range and endurance of the airplane are calculated. The performance module is also capable of calculating the cruise velocity for maximum endurance or maximum range, or simply taking a user input value[10]. The type of propulsion system determines the correct equation to use when calculating the optimum cruise velocity. The altitude lost during the pull-up maneuver is calculated using the deployment flight path angle from the entry trajectory analysis and performing a constant acceleration pull-up maneuver until the airplane reaches level flight.

F. Airplane Communication

The communication analysis computes the power and total energy consumption of the airplane transponder required to transmit the data from the airplane to a relay satellite. The relay satellite can be an existing asset in orbit such as Mars Global Surveyor, the cruise stage inserted into an Aerostationary orbit or a low Mars orbit, or the cruise stage as it flies by Mars. The last of these communication options is only feasible for short duration flights since a line of sight between the cruise stage and airplane exists for a short time period.

G. Airplane Propulsion & Power

This analysis provides five different choices of propulsion system: an NTO/MMH bipropellant rocket, a battery powered propeller, a DMFC powered propeller, a beamed solar powered propeller, and a beamed microwave powered propeller. All of the electric systems share the available power between the subsystems and the primary propulsion system while the rocket propulsion system uses primary batteries to supply electric power to the subsystems.

The bipropellant rocket system consists of a small pressure fed thruster, two propellant tanks, a pressurant tank, feed lines and valves, and primary batteries. Rocket engine mass is based on a curve fit of in-space rocket engines with a thrust range from 4 Newtons to 111 Newtons. The batteries used are the same as the Li/MnO2 batteries used for the battery powered airplane. Propellant mass is computed using the definition of specific impulse and the time of flight.

The remaining propulsion systems are propeller based. These systems share a common propeller efficiency and maximum tip Mach number of 0.85. After the propeller reaches the tip speed limit, an additional propeller is added and the diameter is decreased. The electric motor mass is based on a curve fit of small electric motors with power outputs from 2.3 kW to 11.3 kW. Gearbox mass is added to reduce the rotation rate of the propeller by a factor of two.

The battery system is computed using the energy density of the Li/MnO_2 high discharge rate batteries and the total energy required for the flight. The batteries are packaged assuming cylindrical cells with an additional 10% packaging efficiency loss.

The DMFC system is sized by calculating the cell stack mass based on the power required, and the propellant mass based on the total energy required. The fuel cell stack is based on numbers published by Ballard Power Systems[11], and the combustion efficiency is based on experimental systems at Los Alamos National Labs[12,13]. The stack has a power density of 500 kW/m^3 and an efficiency of 37%.

Both of the beamed power systems calculate a beam power flux density required based on the power required for cruising flight. The airplane then carries the required power conversion system; solar cells or microwave rectennas. The hardware required on the satellite end is calculated in the spacecraft mass analysis.

The solar beamed power system uses an inflatable concentrator on the cruise stage capable of steering to track the airplane on the surface. The inflatable concentrator saves significant mass over a rigid deployable antenna[14], but introduces a dynamics problem due to the flexibility of the structure. The airplane carries solar cells on the wings, tail, and fuselage to convert the concentrated beam of light into electricity at 20% efficiency. Batteries are carried to handle 10% of the flight with a maximum of three hours.

The microwave power system uses a nuclear power source on the cruise stage and a microwave antenna. The antenna operates at 2.45 GHz with a DC to microwave conversion efficiency of 20%. For microwave systems the beam spread is inversely proportional to the antenna diameter, so a large antenna diameter is required to keep the total power requirement low. The rectennas mounted on the wings, tail and fuselage convert the microwave power back to DC at 86% efficiency. The microwave antenna and rectenna are both heavier than their counterparts in the solar powered system.

H. Airplane Mass

The airplane mass analysis sums the masses of the other subsystems, and calculates the mass of the vehicle structure. Parametric mass estimating relationships for unmanned vehicles[15,16] and light-weight aircraft[17] are used to

estimate the structure mass. Adjustments are made where necessary to account for the difference in gravity. Outputs include the gross mass of the airplane, and the power and energy required by subsystems other than communication, propulsion, and the payload.

I. Spacecraft Communication

The spacecraft communication analysis calculates the power and energy required to relay housekeeping, engineering, and science data back to Earth. The analysis assumes one eight hour window per day to communicate with the deep space network using x-band, and then calculates the required data rate based on the payload data rate and the total flight time. When the cruise stage is not used to relay science data back to Earth the data rate is set at a low level to handle housekeeping and engineering data only. The cruise stage side of the UHF communication link to the airplane is also analyzed for power, mass, and volume requirements.

J. Entry System

The entry system scales the geometry of a 70° sphere-cone or a loaf shaped capsule[18], and estimates the mass of the complete entry system. Data from the entry trajectory is used to calculate the required thickness of the SLA-561V heat shield taking into account both ablation and internal temperature limits. The size of the capsule is determined from the folded dimensions of the airplane with ten centimeters added for clearance. The resulting aeroshell mass and outer dimensions are used in launch vehicle selection and the entry trajectory calculation.

K. Entry Trajectory (POST)

The entry trajectory is calculated starting at an altitude of 125 kilometers. The initial velocity is determined using two body orbital mechanics from the conditions at the sphere of influence obtained from IPREP. The entry flight path angle is a user input since this value can be changed using small trajectory correction maneuvers. From the atmospheric interface conditions, POST[19] is used to propagate the entry capsule trajectory. Parachute deployment occurs at Mach 2, and the heatshield and airplane are deployed at subsequent user specified velocities. Outputs include the airplane deployment altitude, the maximum heat rate, the total heat load, and the time from simulation start until the airplane is deployed. This analysis primarily supports the heat shield calculations, but also ensures that the airplane deploys with sufficient clearance above the ground.

L. Spacecraft Mass

The spacecraft mass model uses fixed masses for the avionics, guidance and navigation, and sensors, and parametric models for the power systems, structure, and propulsion system. The propulsion system is sized based on the required velocity changes for both large and small maneuvers. Main engines are only included if a single burn requires a velocity change greater than 500 m/s. Nuclear electric and solar power options are included along with an option for orbit insertion of the cruise stage at Mars. If orbit insertion is not chosen the cruise stage will enter the planetary atmosphere. The spacecraft layout is similar to that used for the ARES and Genesis missions, packaged such that the diameter of the aeroshell is the limiting dimension when configured for launch.

M. Launch Vehicle

The launch vehicle analysis uses the maximum packaged diameter; the spacecraft gross mass, and the required C_3 to select the cheapest launch vehicle capable of performing the mission. The mass and size of the spacecraft provided does not include any contingency, so the launch vehicle is selected based on the current best estimate mass. The launch vehicle database only includes vehicles from the Atlas and Delta families.

N. Cost

The cost model used is a spreadsheet implementation of the NASA Jet Propulsion Laboratory cost model[20]. These cost estimating relationships are derived from planetary spacecraft and provide a good estimate for the cruise stage. The model calculates the life cycle cost for the mission including phases A thru E of the project and includes a 20% reserve on phases A thru D.

Cost numbers are presented in millions of dollars in fiscal year 2004.

III. Airplane Description

The baseline vehicle for this study is based on the ARES study performed at NASA Langley Research Center[21]. The airplane is configured with a swept wing and inverted v-tail. Figure 4 shows the ARES vehicle in the flight configuration. The baseline vehicle has a wingspan of 6.26 m and a planform area of 7 m^2. Propulsion is provided by

a throttled MMH/NTO rocket engine with a specific impulse of 290 s. Electrical power for subsystems is provided by Li/MnO_2 batteries. The communication system uses existing satellites to relay science data back to Earth and the airplane is deployed at subsonic speed during parachute descent of the entry system. A direct entry trajectory with a Viking-like entry capsule is employed.

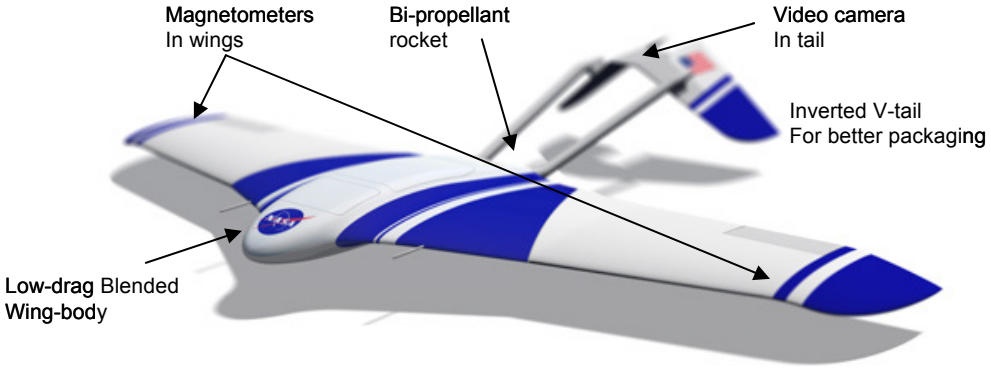

Figure 4. The ARES vehicle configuration shown with key features.

O. Model Validation

When the design variables are set at the values used in the ARES project the subsystem masses compare favorably, but the predicted propellant load is heavier due to the flight profile. For simplicity, the model built for this study uses a constant velocity flight profile, while the ARES team used a constant lift to drag ratio during cruise, leading to a slightly lower propellant mass. Despite these differences, the current model produces an airplane gross mass just 3.3% heavier than ARES' mass estimate. At the mission level, the life cycle cost, wet launch mass, and entry system mass are all within 9% of the ARES values. These errors are well within the accuracy of either system level model.

When optimized for endurance, the result is a vehicle capable of flying for 2.39 hrs, 79% greater endurance than ARES. This longer endurance airplane weighs 296kg, 127% more than ARES. Inclusion of the 30% launch mass margin results in the use of the same launch vehicle, the Delta II 7925.

P. Technology Trades

This study examines the influence of different propulsion systems, different configurations, and different entry systems on the performance of the airplane. These are chosen because of the large dependence of the airplane endurance on the efficiency of the propulsion system, the large influence of aerodynamic performance on endurance, and the difficulty of packaging an airplane in a traditional aeroshell. Five propulsion systems, 2 configurations, and 2 aeroshells are explored. All propulsion system improvements are made from the baseline, and the configuration and aeroshell changes are made independently and together since packaging of the airplane in the aeroshell is highly dependent on the airplane configuration.

The propulsion systems explored are a NTO/MMH bipropellant rocket, a battery powered propeller, a direct methanol fuel cell powered propeller, a beamed solar powered propeller, and a beamed microwave powered propeller.

IV. Modeling Techniques

The optimization problem can be stated in standard form as:

Maximize: Cruise Time
By changing: Range, Pull-up Velocity, C_3 LV, Cruise Velocity
Subject to: $1-n<0$ $W_{folded}-4.8<0$
$V_{cruise}/100-1.8<0$ $Vol_{subs}-Vol_{fuse}<0$
$1.5-(gdalt/1000-D_{pullup}/1000)<0$

The objective function is to directly maximize the airplane endurance, and the design variables are the airplane range, velocity at airplane release, the C_3 provided by the launch vehicle, and the cruise velocity. The four design

variables allow the optimizer to control the endurance of the airplane and to satisfy the constraints. By using the C_3 provided by the launch vehicle as a design variable the optimizer is capable of making the trade between launch vehicle and spacecraft mass. The base constraints listed here set physical limits on the system. The normal force constraint is required when the optimizer is controlling the cruise velocity since maximum endurance is achieved when the velocity is minimized, possibly resulting in less lift than required to maintain level flight.

Three different optimization techniques (user-driven fixed point iteration, partial optimizer based decomposition, and a hybrid method) were attempted during this project due to the poor convergence of the initial model.

Q. User-Driven FPI

For the user-driven FPI formulation the performance analysis optimizes on the cruise velocity to maximize the endurance, and the user changes the three available design variables: range, pull-up velocity, and C_3 provided by the launch vehicle. This is the traditional method of performing system design and is included as a baseline. This method requires that the user enforce the five constraints: pull-up above the ground, aeroshell diameter less than fairing diameter, cruise velocity below Mach 1, available volume greater than required volume, and load factor greater than 1. This method makes use of the knowledge of the designers, but likely will not obtain a solution as close to the constraints as the numerically optimized solutions. A DSM of the Mars airplane problem configured for FPI is shown in Figure 2.

R. Partial OBD

The partial OBD formulation of the problem used 12 design variables, and 13 constraints. Partial OBD calls for the elimination of all optimizers at the discipline level. This moves all design variables to the system level optimizer. The formulation used in this analysis moves all airplane design variables, and most of the mission design variables to the system level optimizer. The mission design variables that were retained at the analysis level were for the interplanetary trajectory analysis and the launch vehicle analysis, neither of which contribute to the objective function, the airplane cruise time. Figure 5 shows a portion of the airplane DSM configured for OBD. If an objective such as minimization of life cycle cost were implemented then the effect of this sub-level optimizer would need to be carefully considered since the two objective functions might conflict.

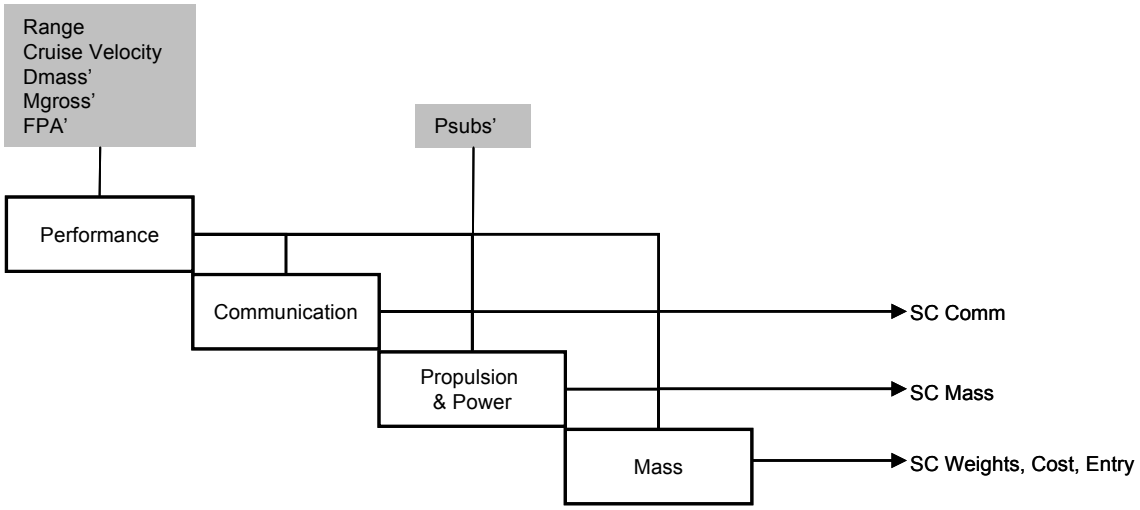

Figure 5. A portion of the Mars airplane analysis DSM configured for OBD. Notice the lack of feedback variables and the increase in optimizer variables. Primed variables (variable') indicate guess variables that must satisfy compatibility constraints. Variables from the optimizer are shown in grey boxes.

S. Hybrid Method

This formulation was conceived after difficulty was encountered trying to implement OBD for this problem. It uses a system level optimizer to control the design variables, and FPI to converge the feedback variables, while keeping the cruise velocity optimizer in the performance contributing analysis. This results in an automated version of the user-driven FPI method which should save considerable run time.

T. Scaling

All of the design variables and constraints are scaled so that they are of order one. Scaling of the constraints was particularly important for this problem because the magnitude of the variables was drastically different.

V. Results

To benchmark each of the optimization methods, each was run from the same starting location. The test case is the ARES like configuration with a bipropellant rocket engine and a 10.1 kg payload. The starting values for the design variables are shown in Table 2. The table is organized to show which variables are design variables for each optimization method.

Table 2. Starting values for the design variables for optimization method comparison. The starting values labeled "Iterative solution" are guessed initially at the same values as for OBD, but are not controlled by the optimizer. The cruise velocity is optimized via an equation in both FPI methods.

	OBD	User-Drive FPI and Hybrid Methods
Range	600 km	600 km
Pull-up Velocity	110 m/s	110 m/s
Cruise Velocity	90 m/s	Equation
C_3 Provided by Launch Vehicle	10 km^2/s^2	10 km^2/s^2
Plane Gross Mass	100 kg	Iterative solution
Plane ΔMass	50 kg	Iterative solution
Power for Subsystems	0.3 kW	Iterative solution
Spacecraft Gross Mass	700 kg	Iterative solution
Total Heat Load	$1x10^6$ J/m^2	Iterative solution
Max Heat Rate	300 kW/m^2	Iterative solution
Time Hot	260 s	Iterative solution
Flight Path Angle at Pull-up	-32°	Iterative solution

It was discovered early in the project that when the optimizer converged, it had not always reached the optimum solution. When restarted it would sometimes run for several more iterations and find a better solution. To ensure that the optimum was reached with the numerically optimized methods the optimizer was restarted each time it stopped. Since the system level optimizer uses SQP, this resets the Hessian matrix that builds up over time, and can become inaccurate relative to the current location.

Figures 6 shows the convergence history for each of the optimization methods starting at the location in Table 2. When using the OBD scheme the solution is obtained in 12 iterations taking about 8 minutes. The final solution is presented in Table 3 along with the other two methods.

The user-driven FPI method converged in 19 iterations taking 41minutes. It should be noted that the user must pay attention to the model for the duration of the run time and change the inputs immediately upon convergence; otherwise the run time will be longer. The solution was significantly better than that of OBD, which will be explored further in the next section. To aid in this discussion Table 4 shows the value of a few key constraints of the converged model.

The hybrid method converged in 6 iterations taking 26 minutes. This was much faster than the user-driven method, and is even more significant when you consider that this model did not require continuous user intervention. The solution, however, is not as good as that of the user-driven method and is significantly better than the OBD solution.

Table 3. The final solution obtained by each of the optimization methods.

	OBD	User-Driven FPI	Hybrid Method
Endurance	1.87 hrs	2.39 hrs	2.19 hrs
Range	869 km	1,461 km	1,246 km
Pull-up Velocity	159 m/s	120 m/s	160 m/s
Cruise Velocity	129 m/s	170 m/s	158 m/s
C_3 Provided by Launch Vehicle	10 km^2/s^2	10 km^2/s^2	10 km^2/s^2
Plane Gross Mass	202 kg	297 kg	250 kg
Plane ΔMass	108 kg	187 kg	148 kg
Power for Subsystems	0.31 kW	0.31 kW	0.31 kW
Spacecraft Gross Mass	606 kg	706 kg	657 kg
Total Heat Load	$1.00x10^6$ J/m^2	$1.12x10^6$ J/m^2	$1.06x10^6$ J/m^2
Max Heat Rate	233 kW/m^2	259 kW/m^2	248 kW/m^2
Time Hot	265 s	308 s	269 s
Flight Path Angle at Pull-up	-32.4°	-26.7°	-32.5°

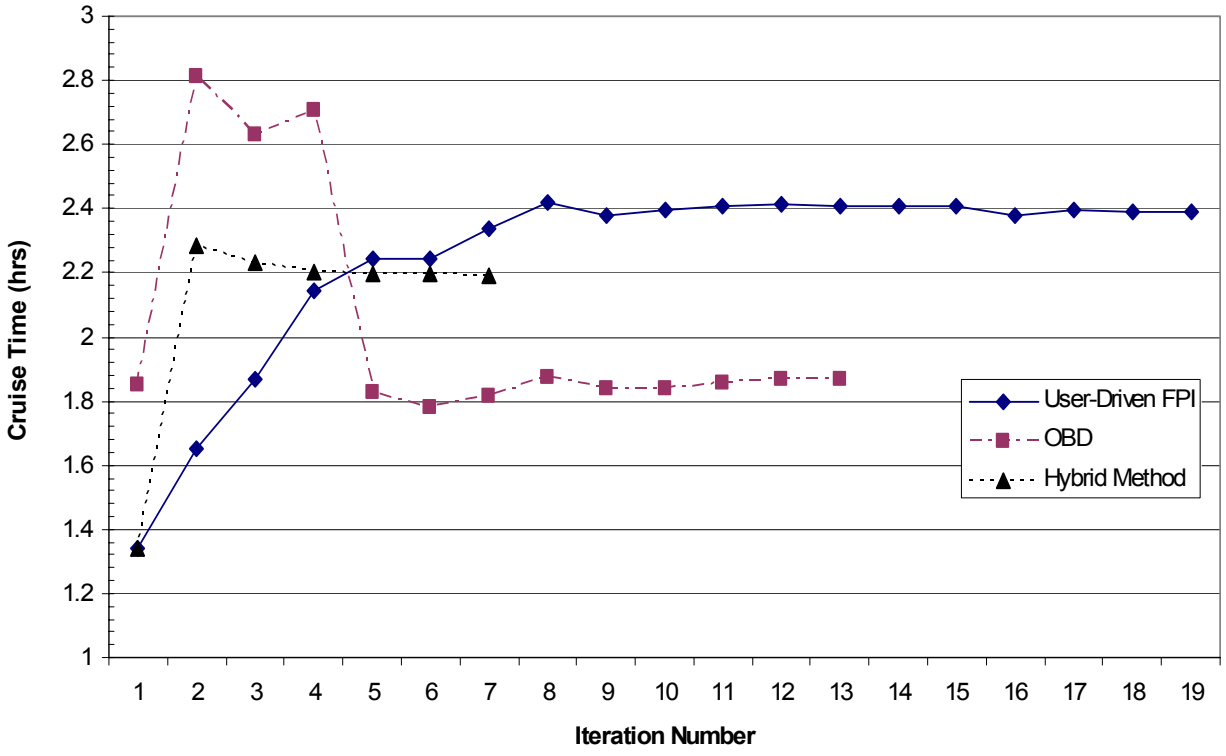

Figure 6. Both numerically optimized methods show the typical pattern of overshoot and then settle to a lower solution, but not the optimal one. The OBD solution starts at a higher value because it does not use the endurance optimized velocity.

Table 4. Selected constraint values of the converged model for each optimization method. All constraints are in standard form where negative values are feasible.

	OBD	User-Driven FPI	Hybrid Method
Volume Constraint	-1.0025	-0.49373	-0.0006
Velocity Constraint	-0.5063	-0.2211	-0.1019
Pull-up Constraint	-4.6989	-2.0808×10^{-5}	-0.4131
Wing Loading Constraint	2.2205×10^{-16}	1.1102×10^{-16}	0.0000

VI. Discussion

The most alarming observation of the above results is the difference in the solutions obtained using the three optimization methods. OBD produces a drastically lower solution than the two FPI based methods. Since the hybrid method (the other gradient based method) obtained an answer much closer to the user-driven method, it seems unlikely that the numerical gradients are fully to blame. The main differences between the numerically driven methods are the number of design variables, and the method of converging the feedback variables. Convergence of the feedback variables is accomplished through compatibility constraints for the OBD scheme. The constraint tolerance in the optimizer is larger than the tolerance that the FPI based methods converge to because a small constraint tolerance results in the optimizer stopping prematurely. A larger tolerance on the feedback variables will typically result in a better solution because the optimizer will use this to its advantage by essentially allowing a solution outside of the constraints. Since the OBD method does not converge the compatibility constraints as tightly, the remaining reason for the lower solution must be the increased number of design variables, poor gradients, or non-linearity in the design space. Due to noise introduced in the FPI convergence, the OBD scheme typically takes more accurate gradients. This leaves the number of variables as the source of the poor solution obtained by OBD or model non-linearity. The number of design variables is significantly larger than for the hybrid method, but is still small compared to problems previously solved[14]. Non-linearity of the model could still be causing problems, though this is difficult to determine without mapping a significant portion of the design space. Furthermore, SQP can theoretically handle non-linear problems. Changes of curvature in the design space might explain why the optimizer sometimes stops prematurely, as rapidly changing gradients can trigger convergence criteria. The difficulties encountered in this analysis cannot be attributed to a single problem. Rather, a combination of the above mentioned problems created the difficulties observed.

The slope of the constraints near the optimum solution also can affect the convergence of numerical optimization methods. Figure 7 shows the wing load factor constraint over a range of the two primary design variables. The range covered does not include the volume constraint, but it should lie just to the right of the data. The wing loading constraint forms a boundary that is very close to the contour lines of the objective function, making it difficult for the optimizer to choose the move direction. This slows the convergence rate of the optimizer once it encounters this constraint, and can even cause the optimizer to think that a converged solution has been found prematurely.

The primary constraint that indicates if a true maximum has been obtained is the volume constraint since this indicates whether the optimizer has filled the airplane with the energy source. A quick look at the volume constraint (Table 4) shows that the hybrid method obtains a solution that is closest to the constraint boundary. The other three constraints indicate the feasibility of the solution from various physical aspects. The velocity constraint is set at 180 m/s, very close to the speed of sound. The pull-up constraint ensures that the airplane is capable of pull-up without impacting the ground, and the wing loading constraint ensures that the lift produced at cruise velocity is at least equal to the airplane weight. All of these constraints are normalized and in standard form such that negative values indicate a satisfied constraint.

The remainder of this study was performed using the hybrid method due to its rapid convergence. After running the hybrid method each solution is adjusted by hand to achieve the best solution possible. Figure 8 shows a comparison of the propulsion systems considered. The DMFC system was determined to be the best system for a long term Mars airplane with an on-board power system, but the solar power system has the potential for indefinite flight. Airplane design aspects of this technology trade study can be found in Rohrschneider, et al[22].

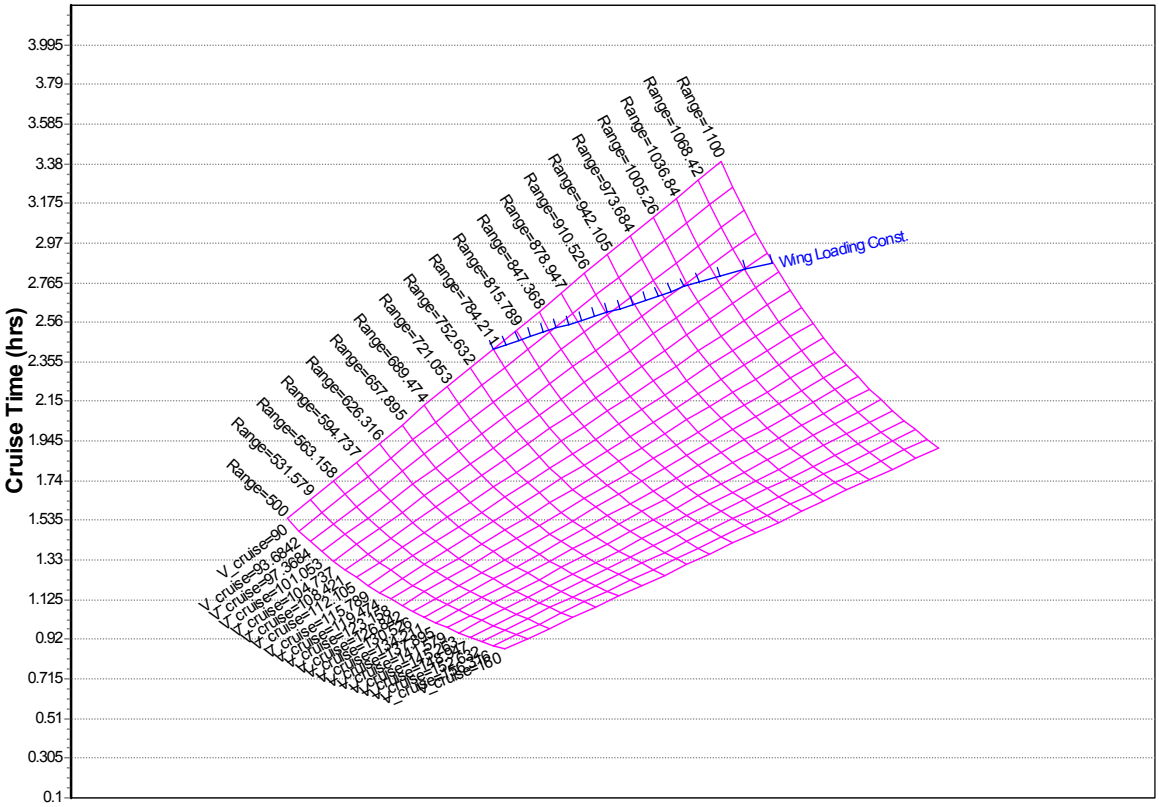

Figure 7. The slope of the wing load factor constraint relative to contour lines of the objective function is shallow as viewed in this carpet plot. The solution is obtained for the bi-propellant airplane at a scale size of 1.5 and a payload of 8.1 kg. The optimum is to the right of the plot data.

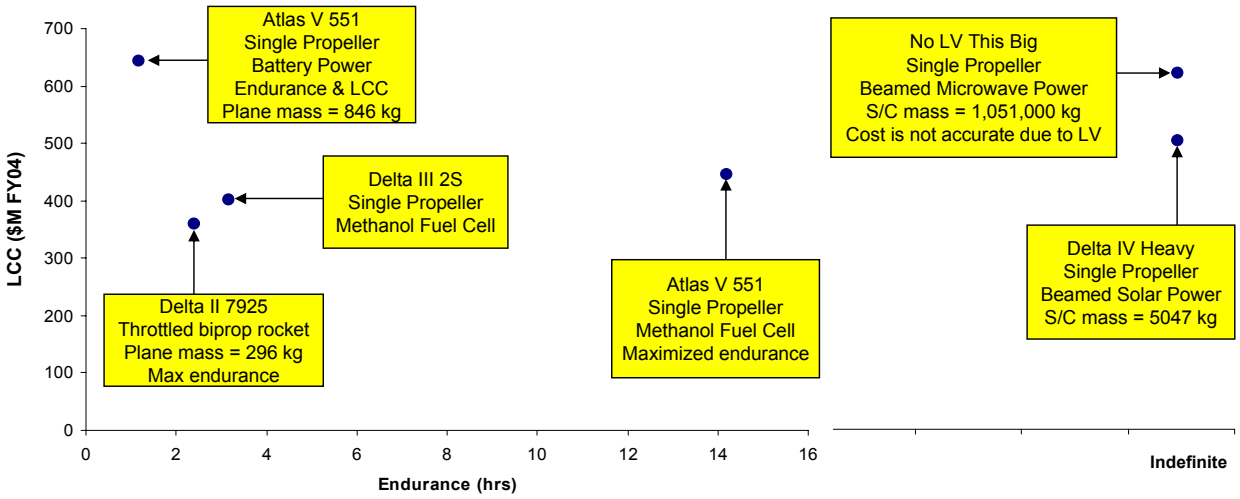

Figure 8. Optimal solutions for each power system option using a combination of the hybrid and user-driven methods.

Due to the low efficiency of the antenna and beam focusing challenges, the microwave system is too massive to be launched on any single current launch vehicle. Preliminary results revealed that the microwave powered airplane mass is similar to that of the solar beamed power airplane, but the cruise stage is much heavier due to the nuclear power system and the microwave antenna. Further analysis of the microwave beamed power system will not be included since the mass of the cruise stage prevents the mission from being launched in one piece on any current launch vehicle. The beamed power systems both require the cruise stage to be placed into an Aerostationary orbit with enough inclination to avoid shading so that the airplane can be powered continuously. To keep a reasonably sized concentrator or antenna the tracking accuracy is required to be within 10m at the airplane. This is a very stringent requirement and is not possible with systems currently employed at Mars. Future orbital assets may enable this tracking accuracy.

The hybrid and user-driven methods work particularly well for this problem because the cruise velocity optimization at the discipline level can be formulated to agree completely with the system level optimizer's objective. If the objective at the system level were to include the life cycle cost (i.e. cruise time/LCC) then the cruise velocity optimizer would need to be reformulated to include the life cycle cost, or the method would produce a suboptimal solution.

VII. Conclusions

The task of optimizing the endurance of an airplane for flight on Mars was undertaken using the design framework ModelCenter, and three different optimization techniques. The traditional user-driven FPI method found a better solution than either of the methods utilizing a numerical optimizer. The formal multi-disciplinary optimization method (OBD) took the least amount of time, but produced the worst solution of the three methods. This appeared to be largely due to a combination of problems including more design variables, model non-linearity, and inaccurate gradients. The convergence difficulties of this model will be explored further in the future. The hybrid method resulted in a solution slightly worse than the user-driven method, but required no human intervention during the analysis. These results lead to the conclusion that the best optimization technique for this problem involves a combination of the two FPI based methods.

References

[1] Clarke, V.C., et al, "Final Report of the Ad Hoc Mars Airplane Science Working Group," NASA CR-158000, 1978.

[2] Cutts, J.A., et al, "Role of Mars Aerial Platforms in Future Exploration of Mars," Draft 10, August 31, 1998.

[3] Braun, R.D., Wright, H.S., Croom, M.A., Levine, J.S., and Spencer, D.A., "The Mars Airplane: A Credible Science Platform," IEEE 1260, *IEEE Aerospace Conference*, Big Sky, MT, Mar. 6-13, 2004.

[4] Levine, J.S., Blaney, D., Connemey, J., Greeley, R., Head III, J., and Hoffman, J., "Science from a Mars Airplane: The Aerial Regional-Scale Environmental Survey (ARES) of Mars," AIAA 2003-6576, *2nd AIAA "Unmanned Unlimited" Conference*, San Diego, CA, Sept. 15-19, 2003.

[5] ModelCenter Ver. 6.0, Design Integration Software, Phoenix Integration, Inc., Blacksburg VA, 2004.

[6] Humble, R.W.(ed.), Henry, G.N.(ed.), and Larsen, W.J.(ed.), *Space Propulsion Analysis and Design: Revised*, Space Technology Series, McGraw Hill Companies, Inc., New York, 1995.

[7] Hong, P.E., Kent, P.D., Olson, D.W., and Vallado, C.A., "Interplanetary Program to Optimize Simulated Trajectories (IPOST). Volume 1: Users Guide," NASA CR-189653-VOL-1-REV, 1992.

[8] Justus, C.G., and James, B.F., "Mars Global Reference Atmospheric Model 2000 Version (Mars-GRAM 2000): Users Guide," NASA TM-2000-210279, 2000.

[9] Guynn, M., Croom, M., Smith, S., Parks, R., and Gelhausen, P., "Evolution of a Mars Airplane Concept for the ARES Mars Scout Mission," AIAA 2003-6578, *2nd AIAA "Unmanned Unlimited" Conference*, San Diego, CA, Sept. 15-19, 2003.

[10] Raymer, D.P., *Aircraft Design: A Conceptual Approach*, 3rd ed., AIAA Education Series, New York, 1999.

[11] Harris, D., "Ballard Extends Industry Lead with Unveiling of Next Generation Fuel Cell," Ballard Power Systems, Inc., Burnaby, BC, Canada, January 9, 2000.

[12] Thomas, S.C., Ren, X., Gottesfeld, S., Zelanay, P., "Direct Methanol Fuel Cells: Progress in Cell Performance and Cathode Research," *Electrochimica Acta*, Vol. 47, No. 22-23, 2002, pp. 3741-3748.

[13] Ren, X., Thomas, S., Zelenay, P., and Gottesfeld, S., "Recent Advances in Direct Methanol Fuel Cells at Los Alamos National Laboratory," *Joint Fuel Cell Technology Review Conference*, Chicago, IL, Aug. 3-5, 1999.

[14] Rohrschneider, R., Sakai, T., Steffes, S., Grillmayer, G., St. Germain, B., and Olds, J., "Solar Electric Propulsion Module Concept for the *BiFrost* Architecture," IAC-02-S.4.09, *53rd International Astronautical Congress, The World Space Congress - 2002*, Houston, Texas, October 10-19, 2002.

[15] Colozza, A.J., "Preliminary Design of a Long-Endurance Mars Aircraft," NASA CR-185243, 1990.

[16] Hall, D.W., Parks, R.W., and Morris, S., "Airplane for Mars Exploration: Conceptual Design of the Full-Scale Vehicle Design, Construction and Test of Performance and Deployment Models," report submitted to NASA Ames Research Center by Dvid Hall Consulting (available at www.redpeace.org/Propulsoin.pdf).

[17] Rohrschneider, R.R., "Development of a Mass Estimating Relationship Database for Launch Vehicle Conceptual Design," Master's Special Project, Georgia Institute of Technology, Atlanta, GA, 2002.

[18] Gage, P.J., Allen Jr., G.A., Park, C., Brown, J.D., Wercinski, P.F., and Tam, T.C., "A Loaf-Shaped Entry Vehicle for a Mars Airplane (The Best Thing Since Sliced Bread?)," AIAA 2000-0634, *38th AIAA Aerospace Sciences Meeting and Exhibit*, Reno, NV, Jan 10-13, 2000.

[19] Brauer, B.L., Cornick, D.E., and Stevenson, R., "Capabilities and Applications of the Program to Optimize Simulated Trajectories," NASA CR-2770, Fegruary, 1977.

[20] Rosenberg, L., "Parametric Cost Modeling of Unmanned Space Projects When the Rules Have Just Changed," Presented at the *First Annual Joint ISPA/SCEA International Conference*, Toronto, Ontario, Canada, June 1998.

[21] Wright, H.S., Croom, M.A., Braun, R.D., Qualls, G.D. and Levine, J.S., "ARES Mission Overview – Capabilities and Requirements of the Robotic Aerial Platform," AIAA 2003-6577, *2nd AIAA "Unmanned Unlimited" Conference*, San Diego, CA, Sept. 15-19, 2003.

[22] Rohrschneider, R.R., Olds, J.R., Kuhl, C.A., Braun, R.D., Steffes, S.R., and Hutchinson Jr., V., "Flight System Options for a Long Duration Mars Airplane," AIAA 2004-6568, *3rd AIAA "Unmanned Unlimited" Technical Conference*, Chicago, Illinois, Sept. 20-23, 2004.